# A laboratory study of the Schmidt number dependency of air-water gas transfer

Kerstin E. Richter[1] and Bernd Jähne[1,2]

[1] *Institute for Environmental Physics, University of Heidelberg, Im Neuenheimer Feld 229 6, 69120 Heidelberg, Germany, E-mail: Kerstin.Richter@iup.uni-heidelberg.de*

[2] *Heidelberg Collaboratory for Image Processing, University of Heidelberg, Speyerer Straße 6, 69115 Heidelberg, Germany, E-mail: Bernd.Jaehne@iwr.uni-heidelberg.de*

**Abstract**. Using a novel fast technique to measure gas transfer velocities, the dependency of gas transfer on the Schmidt number exponent $n$ could be determined with a high precision. It was shown that the transition of $n$ from a smooth ($n=2/3$) to a rough ($n=1/2$) surface extends over a larger range of wind speeds. The *facet model* assumes that an increasing fraction of exchange happens with an exponent of 1/2 and links this fraction with a physical property of the wave field, the mean squared slope $\sigma_s^2$. This new model could be successfully applied to gas exchange rates measurements in two different wind-wave facilities. The geometry of the wind-wave facility used was shown to play a role in the shape of the transition of the Schmidt number exponent.
Key Words: Schmidt number exponent, transfer velocity, facet model

## 1. Introduction

Knowledge of the Schmidt number dependency of the air-sea gas exchange rate $k$, which is given as $k \propto Sc^{-n}$, is incomplete. It is assumed that the Schmidt number exponent $n$ gradually decreases from 2/3 for a smooth to 1/2 for a rough surface. The exact shape of this transition, however, is not known. When the transfer velocity of one tracer $k_1$ is computed from another tracers transfer velocity $k_2$ using the so called *Schmidt number scaling*,

$$\frac{k_1}{k_2} = \left(\frac{Sc_2}{Sc_1}\right)^n \tag{1}$$

the importance of the Schmidt number exponent becomes apparent.

The purpose of this work is twofold. On the one hand, the facet model that describes the transition of the Schmidt number exponent from smooth to rough surface condition is introduced in Section 3. On the other hand, a new scheme for fast and precise measurements of air-sea gas transfer rates in the laboratory is presented in Section 4. In Section 5, measured Schmidt number exponents are

shown and the facet model is applied to this data.

## 2. Theory

According to Fick's law, the flux density $\vec{j}$ of a tracer that is transported by molecular diffusion is proportional to the concentration gradient $\vec{\nabla} c$,

$$\vec{j} = -D\vec{\nabla} c, \tag{2}$$

with $D$ denoting the tracers diffusion coefficient. If there is turbulent transport in addition to diffusion, Eq. (2) needs to be modified by introducing a turbulent diffusion coefficient $K_t$,

$$\vec{j} = -(D + K_t)\vec{\nabla} c. \tag{3}$$

In a stationary and homogeneous case of gas transfer across the air-sea boundary and without sinks and sources by chemical reactions, the flux density $j$ is in vertical direction and constant. Eq. (3) simplifies to

$$\frac{1}{k} := \frac{c(z_r) - c(0)}{j} = \int_0^{z_r} \frac{1}{D + K_t(z)} dz \tag{4}$$

with $k$ denoting the transfer velocity. Before integrating this equation the turbulent diffusion coefficient $K_t$ needs to be investigated. Far away from the interface it is set to be proportional to the distance from the interface $z$, $K_t \propto z$ (Jähne 2009). Closer to the interface the turbulent motion is attenuated by viscosity. The degree of attenuation depends on the properties of the interface. At a free water surface it ranges from $K_t \propto z^2$ to $K_t \propto z^3$ (Jähne 2009). Integrating Eq. (4) yields

$$k = \frac{u_*}{\beta_s} Sc^{-2/3} \qquad \text{for a smooth water surface} \tag{5}$$

and

$$k = \frac{u_*}{\beta_w} Sc^{-1/2} \qquad \text{for a wavy water surface} \tag{6}$$

with the friction velocity $u_*$, a measure for the momentum transfer across the interface and the resistance for momentum transfer $\beta_s$ and $\beta_w$. $Sc = \nu/D$ denotes the Schmidt number, the ratio of kinematic viscosity of water $\nu$ and the tracers diffusivity $D$. More thorough derivations of Eq. (5) and Eq. (6) can be found in Deacon (1977), Jähne (1980), Coantic (1986) and Yaglom and Kader (1974).

## 3. The facet model

Both cases of a smooth ($n=2/3$) and a wavy ($n=1/2$) surface that were introduced in the previous section rely on the assumption that the respective boundary condition must be fulfilled for the whole surface all the time. However, gas transfer is an intermittent process (Jähne *et al*. 2007). Studies in windwave

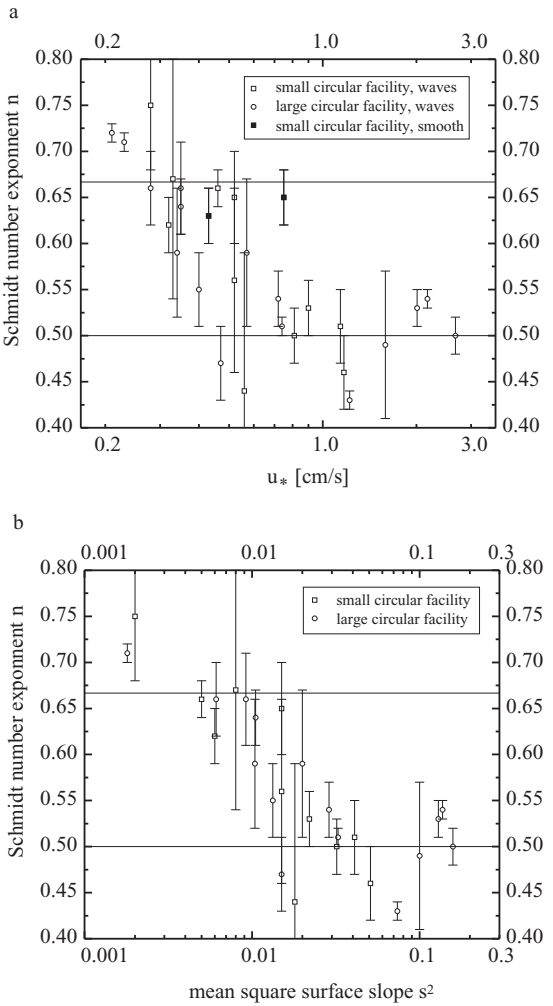


**Figure 1** Plots of the Schmidt number exponent $n$ versus **a** the friction velocity $u_*$ and **b** the mean squared wave slope $\sigma_s^2$ (Jähne *et al*. 1987).

tanks suggested that the transition from flat to rough surface conditions is smooth rather than sudden, see for example Figure 1.

Therefore it is reasonable to part the total water surface into a fraction $A_w$ where the gas transfer is enhanced by waves and a smooth fraction $1-A_w$. The total gas transfer rate can then be calculated by

$$k=A_w\frac{u*}{\beta_w}Sc^{-1/2}+(1-A_w)\frac{u*}{\beta_s}Sc^{-2/3}. \tag{7}$$

(Zappa *et al*. 2002) were able to quantify a fractional area where microscale wave breaking occurs using infrared imagery in a lab study. They showed that the gas transfer rate is linked to this area.

The facet model relates the fractional area $A_w$ to a physical property of the wave field, the surface roughness which is mathematically described as the mean squared slope $\sigma_s^2$,

$$A_w(\sigma_s^2)=\frac{(\sigma_s^2)^\gamma}{\delta^\gamma+(\sigma_s^2)^\gamma}. \tag{8}$$

According to Jähne *et al*. (1985), $\sigma_s^2$ is a quantity that suitably characterizes the boundary conditions of the free water surface. Eq. (8) is further motivated by the assumption, that waves increase surface roughness as well as near-surface turbulence which in turn enhances gas transfer. The free empiric parameter $\gamma$ controls the steepness of the transition. The second free empiric parameter $\delta$ is the value of the mean squared slope, where the surface is equally parted into smooth and rough patches. $\beta_s$ has a theoretically fixed value of 12.2 (Jähne *et al*. 1979), while $\beta_w$ needs to be determined in experiments by regression to transfer velocities at high wind speeds. The shape of the transition of the boundary conditions for $\delta = 0.4$ and three different steepness parameters is shown in Figure 2.

## 4. Experiments

Simultaneous measurements of the transfer velocities $k_1$ and $k_2$ of 2 different tracers can be used to calculate the Schmidt number exponent using Schmidt number scaling Eq. (1),

$$n=\frac{\ln\left(\frac{k_1}{k_2}\right)}{\ln\left(\frac{Sc_2}{Sc_1}\right)}=\frac{\ln\left(\frac{k_1}{k_2}\right)}{\ln\left(\frac{D_1}{D_2}\right)} \tag{9}$$

with the two tracers' Schmidt numbers $Sc_1$ and $Sc_2$ and their diffusivities $D_1$ and $D_2$.

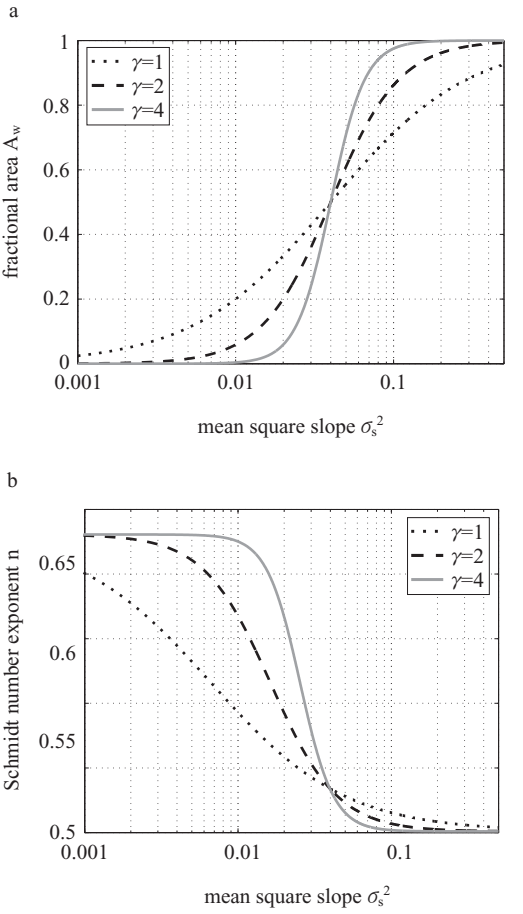


**Figure 2** Predicted shapes of the transition of **a** the fractional area and **b** the Schmidt number exponent for $\delta=0.4$, $Sc=600$, $\beta_s=12.2$, $\beta_w=6$ and three different steepness parameters $\gamma$.

### *4.1 The controlled leakage method*

Figure 3a shows a simplified model of the air and water space of a wind-wave facility. At the start of an experiment slightly soluble tracers are dissolved in the water and their concentrations $c_w$ and $c_a$ in the water volume $V_w$ and air volume $V_a$ are monitored (evasion experiment). Looking at mass balances in the air as well as in the water yields a system of coupled differential equations,

$$V_a\dot{c}_a = kA(c_w - \alpha c_a) \tag{10}$$

$$V_w\dot{c}_w = -kA(c_w - \alpha c_a). \tag{11}$$

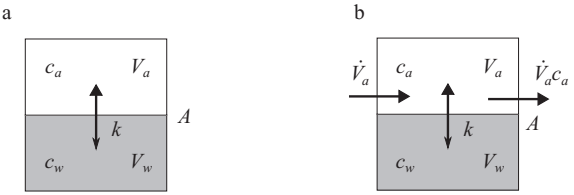


**Figure 3** Box models of experiments **a** without and **b** with a leak.

These equations describe the evasion of a tracer with dimensionless solubility $\alpha$ across the water surface $A$ and can be used to calculate the tracer's transfer velocity $k$. However, time constants of the described evasion experiment lie in the order of many hours or days, depending on the characteristics of the wind-wave facility and the tracer, the wind speed and surfactant coverage.

In Figure 3b the air space is flushed with fresh air at a known flush rate $\lambda_f = \frac{\dot{V}_a}{V_a}$. Eq. 10 is modified,

$$V_a \dot{c}_a = kA(c_w - \alpha c_a) - \dot{V}_a c_a \tag{12}$$

$$V_w \dot{c}_w = -kA(c_w - \alpha c_a). \tag{13}$$

Solving Eq. (12) for the transfer velocity yields

$$k = \frac{V_w}{A} \frac{\lambda_f c_a}{\delta_v c_w} \frac{\lambda_f + \dot{c}_a / c_a}{\lambda_f} \frac{1}{1 - \alpha c_a / c_w}, \tag{14}$$

with $\delta_v = V_w / V_a$, the ratio of water and air volume. To measure the flush rate $\lambda_f$ a tracer that is insoluble in water is given into the air space with a known constant input rate $\dot{V}_f$. In equilibrium, as much tracer is flushed out of the air space as is replaced by the input. When the tracer's air side concentration $c_f$ is measured (in [ppm]), the flush rate can be calculated,

$$\lambda_f = \frac{\dot{V}_f}{c_f V_a}. \tag{15}$$

The time constant of this process is significantly shorter than in the unflushed case. Solving the system of differential equations (Eq.12 and 13) shows that it lies in the order of the time constant of the flushing. Using a high flush rate, the time constant can be as low as some minutes. Therefore this new technique allows very fast measurements of the transfer velocity.

### *4.2 Experimental setup*

The measurements presented in this study were performed in two different

**Table 1** Summary of the features of both annular wind-wave tanks used in this study. *SCWWF* denotes the small circular wind-wave facility.

| | *Aeolotron* | *SCWWF* |
|---|---|---|
| mean perimeter (length) [m] | 29.2 | 3.13 |
| outer diameter [m] | 9.92 | 1.188 |
| inner diameter [m] | 8.68 | 0.802 |
| total height [m] | 2.40 | 0.415 |
| maximum water depth [m] | 1.20 | 0.112 |
| water volume at max. water depth [$m^3$] | 20.7 | 0.07 |
| water surface area [$m^2$] | 18.0 | 0.625 |
| air volume at max. water depth [$m^3$] | 22.7 | 0.230 |
| ratio of water to air volume | 0.91 | 0.30 |

annular wind-wave facilities, the Heidelberg *Aeolotron* and the *SCWWF* (formerly at Woods Hole Oceanographic Institution; 1998-2008 at Univ. of Heidelberg; now at Univ. of Hamburg). Both are detailled in Table 1.

Tracers used were $N_2O$, $CF_2Cl_2$ (CFC-12), He and $H_2$. Gas concentration measurements were performed using a Hewlett Packard *MicroGC* for the lighter molecules (He and $H_2$) and a nondispersive infrared analyser *URAS-14* manufactured by ABB for the other tracers.

In addition the friction velocity $u_*$ was measured using a momentum balance method described in (Nielsen 2004). The mean squared slope $\sigma_s^2$ was measured with a color imaging slope gauge (CISG). Details on the CISG can be found in (Rocholz 2008).

All measurements where conducted at a clean water surface, wind speeds ranging from less than 1 up to 10m/s.

## 5. Results and discussion

Figure 4 shows the measured transfer velocities versus the mean squared slope. While there is a good correlation between the *SCWWF* data and the mean squared slope, a distinct bend can be seen for the *Aeolotron* data at a $\sigma_s^2$ of around 0.01. This is due to inaccurate measurements of the mean squares slope at slopes lower than 0.01, see (Fuß 2004). Therefore, data with a mean squared slope of less than 0.01 was ommitted in further analysis of the *Aeolotron* data. At higher $\sigma_s^2$, the transfer velocities measured in the *SCWWF* are higher than in the *Aeolotron*. On the one hand, deviations in measured transfer velocities are to be expected due to the different geometries of both facilities used. In the smaller *SCWWF* the secondary currents, which are induced by centrifugal forces, are stronger due to the tighter curvature of the walls. These currents provide another source of surface

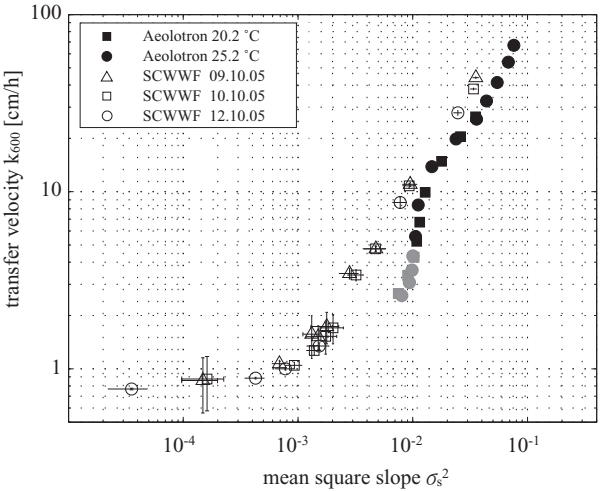


**Figure 4** Transfer velocities scaled to Schmidt number 600 versus mean squared slope measured in the *Aeolotron* (solid symbols) and the small circular windwave facility (*SCWWF*, open symbols). Data of the *Aeolotron* data set with inaccurate mean squared slope is marked in gray.

renewal and thus enhance gas transfer. On the other hand, in the *SCWWF* the mean squared slope was only measured in alongwind direction. The crosswind component was estimated from measurements in other wind-wave facilities, see (Degreif 2006). The total mean squared slope acquired in this way seems to be underestimated.

Figure 5 summarizes the measured Schmidt number exponents. Both data sets show a smooth transition between the rough and the smooth case that extends over a wide range of wind speeds. There is a systematic deviation in all measured Schmidt number exponents of about $-0.05$ in the *Aeolotron* data. This is most likely due to inaccuracies in the diffusion coefficients that where used in evaluating this data set. There is, however, a significant difference between both data sets. This can be explained by the different geometries of the wind-wave tanks. Because of the enhancement of gas transfer due to secondary currents especially in the smaller *SCWWF*, the transition of the Schmidt number exponent starts at lower mean squared slope in this wind-wave facility.

Also shown in Figure 5b is the fit of the facet model to the *SCWWF* data. The transition of the Schmidt number is well described by the model in this data set. The deviation from the model is less than 5%. Due to the already mentioned problems with the mean squared slope measurement, the facet model could not be reliably fitted to the *Aeolotron* data.

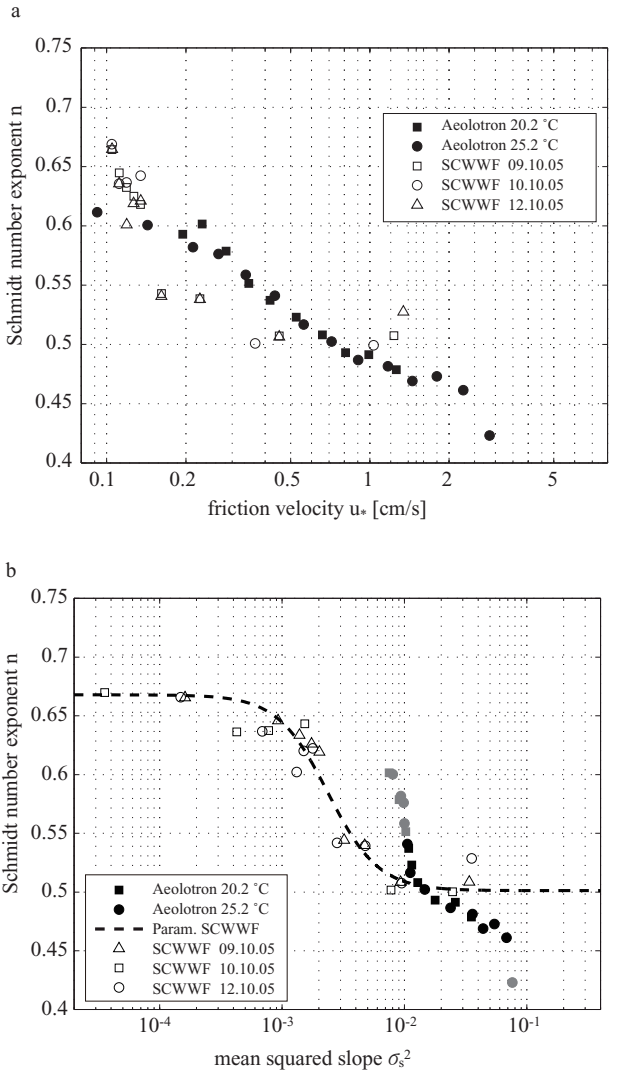


**Figure 5** Schmidt number exponent versus **a** friction velocity and **b** mean squared slope measured in the *Aeolotron* (solid symbols) and the *SCWWF* (open symbols). Also shown is the predicion of the facet model for the *SCWWF* data (dashed line). Data of the *Aeolotron* data set with inaccurate mean squared slope is marked in gray.

## 6. Conclusions

The facet model that describes the transition of the Schmidt number exponent from a flat to a rough water surface was introduced. This model was applied to measurements of the Schmidt number exponent. The transition was found to be smooth and extends over a wide range of wind speeds. However, the geometry of the wind-wave facility used plays a role in the exact shape of this transition. The facet model is capable of modeling the transition.

**Acknowledgements**

We gratefully acknowledge the financial support provided by the German Federal Ministry of Education and Research (BMBF) within the project SOPRAN (contract 03F0462F) - Surface Ocean Processes in the Anthropocene. We would like to thank Kai A. Degreif and Reinhard Nielsen for conducting the measurements.

**References**

Coantic, M. (1986), A model of gas transfer across air-water interfaces with capillary waves, *Journal of Geophysical Research, 91*, 3925-3943.

Deacon, E. L. (1977), Gas transfer to and across an air-water interface, *Tellus*, *29*, 363-374.

Degreif, K. (2006), *Untersuchungen zum Gasaustausch - Entwicklung und Applikation eines zeitlich aufgelösten Massenbilanzverfahrens*, Dissertation, Institut für Umweltphysik, Fakultät für Physik und Astronomie, Univ. Heidelberg.

Fuß, D. (2004), *Kombinierte Höhen- und Neigungsmessung von winderzeugten Wasserwellen am Heidelberger Aeolotron*, Dissertation, Institut für Umweltphysik, Fakultät für Physik und Astronomie, Univ. Heidelberg, Heidelberg, Germany.

Jähne, B. (1980), *Zur Parametrisierung des Gasaustauschs mit Hilfe von Laborexperimenten*, Dissertation, Institut für Umweltphysik, Fakultät für Physik und Astronomie, Univ. Heidelberg, IUP D-145.

Jähne, B. (2009), Air-sea gas exchange, in J. H. Steele, K. K. Turekian, and S. A. Thorpe (Eds.), *Encyclopedia Ocean Sciences*, pp. 3434-3444, Elsevier, invited.

Jähne, B., K. O. Münnich, R. Bösinger, A. Dutzi, W. Huber, and P. Libner (1987), On the parameters influencing air-water gas exchange, *J. Geophys. Res*., *92*, 1937-1950.

Jähne, B., K. O. Münnich, and U. Siegenthaler (1979), Measurements of gas exchange and momentum transfer in a circular wind-water tunnel, *Tellus*, *31*, 321-329.

Jähne, B., C. Popp, U. Schimpf, and C. Garbe (2007), The inuence of intermittency on air/water gas transfer measurements, in C. S. Garbe, R. A. Handler, and B. Jähne (Eds.), *Transport at the Air Sea Interface*, Springer-Verlag.

Jähne, B., T.Wais, L. Memery, G. Gaulliez, L. Merlivat, K. O. Münnich, and M. Coantic (1985), He and Rn gas exchange experiments in the large wind-wave facility of IMST, *J. Geophys. Res*., *90*, 11,989-11,998.

Nielsen, R. (2004), *Gasaustausch - Entwicklung und Ergebnis eines schnellen Massenbilanzverfahrens zur Messung der Austauschparameter*, Dissertation, Institut für Umweltphysik, Fakultät für Physik und Astronomie, Univ. Heidelberg.

Rocholz, R. (2008), *Spatiotemporal Measurement of Short Wind-Driven Water Waves*, Dissertation, Institut für Umweltphysik, Fakultät für Physik und Astronomie, Univ. Heidelberg.

Yaglom, A. M. and B. A. Kader (1974), Heat and mass transfer between a rough wall and turbulent fluid flow at high reynolds and peclet numbers, *J.Fluid Mech*., *62*, 601-623.

Zappa, C. J., W. E. Asher, A. T. Jessup, J. Klinke, and S. R. Long (2002), Effect of microscale wave breaking on air-water gas transfer, in E. Saltzman, M. Donelan, W. Drennan, and R. Wanninkhof (Eds.), *Gas Transfer at Water Surfaces, Geophysical Monograph*, vol. 127, pp. 23-29, American Geophysical Union.